Physica Medica 67 (2019) 91–99

Contents lists available at ScienceDirect

Physica Medica

journal homepage: www.elsevier.com/locate/ejmp

Original paper

Practical implementation of robust MR-thermometry during clinical MR-guided microwave ablations in the liver at 1.5 T

K.R. Gorny[a,*], C.P. Favazza[a], A. Lu[a], J.P. Felmlee[a], N.J. Hangiandreou[a], J.E. Browne[a], W.S. Stenzel[a], J.L. Muggli[b], A.G. Anderson[c], S.M. Thompson[a], D.A. Woodrum[a]

[a] Department of Radiology, Mayo Clinic College of Medicine, Rochester, MN, United States
[b] Department of Anesthesiology and Perioperative Medicine, Mayo Clinic College of Medicine, Rochester, MN, United States
[c] Philips Healthcare, Gainesville, FL, United States

ARTICLE INFO

Keywords:
MR-guided microwave ablations
MR-thermometry
Quality assurance
Artifact reduction
Interventional MRI

ABSTRACT

Practical non-invasive equipment modifications and effective acquisition methods to achieve robust and reliable real-time MR thermometry for monitoring of clinical hepatic microwave ablations were implemented. These included selection of the microwave generator location (inside versus outside the MR scan room), the number of radiofrequency chokes added to the microwave generator's coaxial lines, and the use of copper wool to maximize their electrical grounding. Signal-to-noise ratio (SNR) of MR thermometry images of a small fluid-filled phantom acquired during activation of microwave antenna were used to evaluate image quality as a function of each modification. SNR measurements corresponding to both locations of the microwave generator were comparable and so it was located outside the MR scan room. For this location, addition of one RF choke on the power and four chokes on the sensor coaxial lines was found to be optimal, corresponding to a 68% increase in SNR. Furthermore, image quality strongly depended on the proper electrical grounding of the power and sensor lines. SNR ratio (relative to SNR of baseline images) during activation of microwave generator was found to be 0.49 ± 0.28 without adequate grounding, and 0.88 ± 0.08 with adequate grounding ($p = 0.002$, Student's *t*-test). These SNR measurements were sufficiently sensitive to detect issues related to equipment performance and hence formed part of the quality assurance testing performed prior to each clinical treatment. Incorporating these non-invasive approaches resulted in significant improvements to image quality and, importantly while maintaining the clinical integrity of the microwave system which is of paramount importance in a highly regulated healthcare environment.

1. Introduction

Percutaneous microwave ablations (MWA) of hepatic tumors have been gaining the attention of interventional practices due to the ability to produce large thermal ablations in a variety of different tissues while being relatively immune to the heat-sink effects of large vessels [1,2]. MWA treatments require precise delivery of the treatment applicator (microwave antenna) into target tumor tissues and therefore, rely heavily on image guidance, which has traditionally been accomplished using ultrasound (US) [3] or computed tomography (CT) [4,5]. Recently, magnetic resonance imaging (MRI), which provides superb soft tissue contrast and tumor delineation, has been shown to be advantageous for both precise guidance of antennae placement and accurate assessment of ablation coverage [6,7].

Real- or near real-time thermal monitoring of the MWA progression is clinically desirable to minimize patient risks, particularly when rapid ablations are performed in the vicinity of sensitive healthy tissues. It may also be advantageous when ablation may be sub-optimal and on-the-fly adjustments to treatment parameters are required. While currently US or CT are not capable of providing thermal monitoring during treatments [8–11], MRI offers various approaches for rapid visualization of growing ablation margins [12], with the most widely used approach being proton-resonance-frequency-shift (PRFS) thermometry [12]. In this method, a gradient-echo sequence is executed during the ablation and a series of phase images are reconstructed from the MR data and subtracted from the baseline image acquired prior to start of ablation. At every sampling interval the temperature elevation maps are computed together with the corresponding thermal dose maps derived based on the temperature history of each image voxel up to that point [13]. The assumption behind the reference-based PRFS method is that

* Corresponding author at: Department of Radiology, Mayo Clinic College of Medicine, 200 1st Street SW, Rochester, MN 55905, United States.
E-mail address: gorny.krzysztof@mayo.edu (K.R. Gorny).

https://doi.org/10.1016/j.ejmp.2019.10.020
Received 17 June 2019; Received in revised form 1 October 2019; Accepted 4 October 2019
Available online 06 November 2019

the visualized anatomy is stationary and any phase change between the subtracted images results entirely from changes of temperature. Consequently, PRFS thermometry performs well in the relatively stationary tissues such as uterus [14] or brain [15]; however, it is prone to artifact near moving organs such as the liver. This method may further be affected by increases in electronic noise and electromagnetic interference (EMI) caused by activation of the treatment applicator [16,17]. In our practice, PRFS thermometry is accomplished with the aid of a commercial system (Visualase, Medtronic, Minneapolis, MN) which is FDA-cleared for MRI-guided laser ablations. During activation of microwave system the PRFS sequence is run on MRI scanner and the phase images are transferred to the Visualase workstation every 6–10 s (depending on sequence parameters) where temperature and the resulting binary tissue kill overlays are computed and superimposed as a color map onto the patient's anatomy.

To date, real-time PRFS-thermometry during hepatic MWA has been implemented on open MRI systems using microwave equipment operating at 2.45 GHz: clinically on 0.5 T [18,19] and in animal experiments on 1.0 T [20]. Same microwave system was also used in phantom and animal experiments performed at 7.0 T [21]. With exception of the latter each of these studies reported significant elevations of noise levels and EMI in MR images caused by the action of the microwave generator. In our practice MR-guided MWA treatments are performed using a commercially available MRI-configured microwave AveCure system (MedWaves Inc., San Diego, CA) operating at 902–928 MHz, inside a 1.5 T diagnostic horizontal bore scanner (Ingenia, Philips Healthcare, Best, Netherlands). The AveCure system in similar configuration has previously been used in MWA of ex-vivo porcine livers [22]. In that study the MR-monitoring was accomplished using the temperature-related signal changes in T1-weighted images. To limit effects of increases in image noise and EMI caused by the microwave generator (MWG), the imaging in this study was performed only when the generator was intermittently paused, resulting in temporal resolution on the order of 60 s. For our practice this particular implementation was not satisfactory as the 60-second temporal resolution was deemed insufficient and it is not clear how periodic interruptions to the ablation would affect the therapy. In addition, T1-based thermometry is known to underestimate the size of the thermal dose [23].

Our initial clinical MR-guided MWA were performed with the AveCure generator operated from inside the scanner room. The parameters of the PRFS sequence were adjusted in an attempt to automatically synchronize image acquisitions with the anesthesia-set patient respiration. Despite the adjustments, the PRFS thermometry acquired during MWA was frequently not clinically usable, see Fig. 1 (The de-identified patient images contained in the manuscript were acquired in the course of the retrospective image review study deemed to be exempt from the requirement of approval by our Institutional Review Board. All patients granted access to use of their data). The microwave system introduced a significant amount of noise and EMI which, coupled with the artifacts caused by the patient's respiratory motion, completely obscured the temperature change and thermal dose information rendering the real-time PRFS feedback unusable.

The experience described above motivated the overall goal of the work described in this report, which is to optimize equipment configuration and set-up to provide clinically robust and reliable real-time PRFS thermometry for our clinical microwave hepatic ablation practice. The clinical requirements related to both patient and MRI safety concerns dictated several significant constraints for any changes we implemented within this quality improvement project.

Constraint 1: Due to MRI-safety and workflow concerns associated with limited available space inside MR scan room, MWG placement outside the MR scan room was strongly preferable. For that location, the only viable method of introducing the microwave coaxial lines into MR scan room is via the waveguide through the grounded penetration panel. This in turn could potentially result in significant additional degradation of image quality as the lines extending outside the Faraday cage shielding MR scan room could act as antennae leaking RF noise or EMI. Using similar approach for the purpose of clinical MWA in the prostate, threefold reductions in image SNR and significant degradation of MR thermometry have been reported [27]. To mitigate this issue we established a process (described in the Methods) of electrical grounding of the coaxial cables to the waveguide with coupled with the corresponding SNR testing (intended to be performed prior to treatment).

Constraint 2: Since AveCure is an FDA-approved MWA system whose antennae are inserted into patients percutaneously and come in contact with the blood stream, only non-invasive modifications to the equipment could be considered (e.g. we could not consider in-line RF pass-through or notch filters). Invasive modifications could degrade patient safety and result in voiding of the FDA-approval.

Constraint 3: Hepatic MWA can be rapid and is frequently performed near sensitive non-target tissues. Therefore temporal resolution of MR thermometry was clinically required to be less than 10 s. As the typical acquisition time of one image frame is on the order of 3 s, this precluded us from using any significant signal averaging to address SNR limitations.

Constraint 4: Modifications to MR thermometry acquisition protocol should not require periodic pausing in the microwave ablations. This approach, reported previously [22,27], could potentially have a negative impact on the effectiveness of the MWA therapy.

Our goal in this manuscript is to describe practical, technical

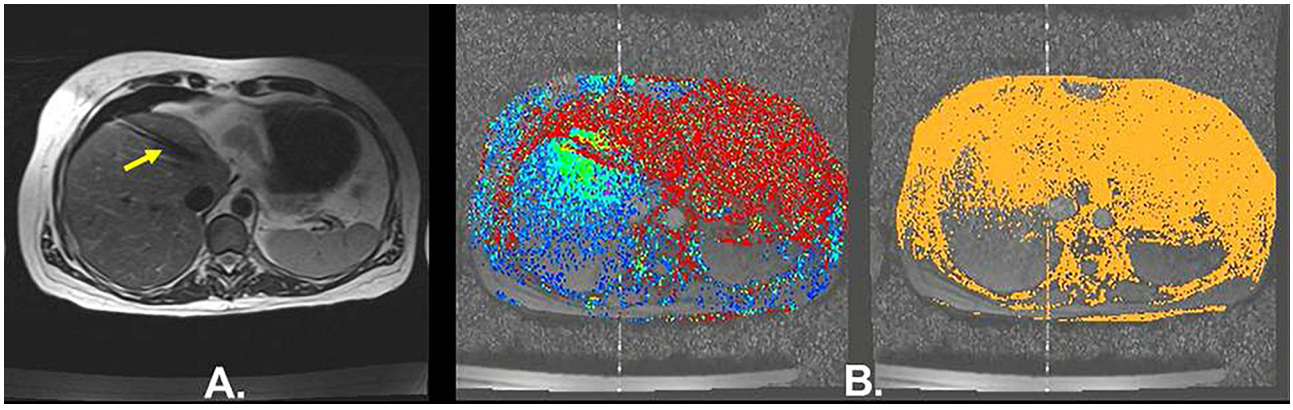

Fig. 1. Challenges of PRFS-thermometry during hepatic MWA. A. Axial T2 image through the liver. Microwave antenna is indicated with an arrow. B. Phase difference (left) and the corresponding thermal damage (right) overlays displayed on the Visualase workstation 3-minutes into the 10-minute ablation. Here the thermal lesion was obscured due to combination of severe noise, EMI (straight vertical lines), and effects of respiratory motion. Note the severe respiratory artifact in the anterior (upper) portion of the anatomy due to both the recoil of the ribcage and tissue heterogeneity. Also, the SNR in the posterior portion is slightly elevated due to higher signal from patient kidneys.

measures and non-invasive equipment modifications that can be made in the clinical environment to allow robust real-time PRFS thermometry, and utilize them for monitoring of MR-guided microwave hepatic ablation procedures while ensuring that this clinical environment still meets all regulatory requirements for patient and staff safety. To our knowledge this study describes the first routine implementation of real-time PRFS thermometry for clinical MR-guided microwave ablation of liver lesions, performed at 1.5 T; this was achieved by a combination of safe equipment modifications and a newly developed pre-procedural quality assurance program.

2. Materials and methods

2.1. SNR measurement setup

All experiments were performed using the MRI-configured AveCure system (MedWaves Inc., San Diego, CA), inside the MRI suite hosting a 70 cm diameter bore 1.5 T scanner (Ingenia, Philips Healthcare, Best, Netherlands). The AveCure system consists of a 902–928 MHz MWG and a set of MRI-safe antennas, which are classified based on their expected ablation coverage: large (4.0 × 5.5 cm in 10 min, 120 °C and 36 W), medium (3.5 × 4.0 cm in 10 min, 120 °C, and 30 W), and small (2.5 × 3.0 cm in 7.5 min, 110 °C, and 28 W). Each antenna has an integrated temperature sensor which is connected to the generator via the "sensor line" which is separate from the "power line". During the ablation, based on the thermal feedback and the measured reflected power, the generator output frequency and power duty cycle are automatically adjusted to optimize antenna performance as tissue conditions changed.

Technical assessments were performed inside the interventional MRI suite with the setup designed to mimic patient treatment, shown in Fig. 2a. A large microwave (MW) antenna was inserted vertically through a fitted Styrofoam cap into a cylindrical container filled with saline located next to the custom-made "small sample noise" phantom consisting of a small cylindrical glass vial (2.5 cm in diameter, 6.0 cm in length) filled with a solution of 0.05 g/L MnCl2 and 2.5 g/L NaCl mixed with 1 cm3/L CH2O (formaldehyde), see Fig. 2b. The small sample noise phantom is routinely used in our practice for troubleshooting issues related to EMI. Its relatively small volume results in maximizing the receiver amplification yet it is sufficiently large for the MRI scanner to reliably set appropriate RF transmit power for imaging. The phantom was positioned in the center of the clinical 20 cm-diameter dStream Flex L Coil (InVivo Corp., Gainesville, FL), see Fig. 2b. All modifications to the microwave system were studied using signal-to-noise ratio (SNR) in the images of the small sample noise phantom acquired with the clinical MR-thermometry protocol during activation of the microwave antenna ("ablation on"), see Fig. 2d. The saline phantom was selected to ensure consistency of microwave ablation parameters during all experimental trials, as saline properties do not change between antenna activations.

2.2. SNR measurement protocol

MR images were acquired with our clinical PRFS protocol (2D spoiled gradient echo: TR = 23 ms, TE = 15 ms, Flip = 15°, matrix = 256 × 256, FOV = 24 × 24 cm, BW = 91 Hz/Px, slice = 5 mm) using a clinical coil setup of a single-channel 20 cm diameter dStream Flex L Coil (InVivo Corp., Gainesville, FL) combined with the 12-channel integrated FlexCoverage Posterior coil (Philips). Each equipment modification was followed by a set of three SNR measurements corresponding to "baseline" (i.e. no microwave equipment inside MR scan room), and "off" and "ablation on" operational modes of MWG. Image signal and noise were measured in the MR images, as shown in Fig. 2d. Mean and standard deviation values of the SNR measurements were computed from subsequent 30 images in the sequence. The time to acquire the sequence of 30 images was 1 min 36 s.

2.3. MWG location

Two potential MWG locations were evaluated using the above SNR measurement approach: one inside and the second outside the scanner room (see Fig. 2a). Inside the MR scanner room the magnetic field maps provided by the scanner vendor-provided were used to ensure the generator was positioned at location where the field was below 1 Gauss. The field and spatial field gradients were additionally measured with direct Gauss meter measurements (F.W. Bell Model 6010, Bell Technologies Inc., Pomona, CA), according to methods described previously [24]. Since the generator functions are controlled manually, during use inside the scanner room the operator was required to wear ear protection and communicate with the technologist at the scanner console via the intercom. For the location outside the scanner room (the "workroom", see Fig. 2), the antenna's power and sensor lines were connected to MWG through a waveguide in the penetration panel.

2.4. Addition of RF chokes

Low-pass filters (< 100 MHz) in the form of ferrite RF chokes (Laird PLC, London, UK) were incrementally added onto the power (Part Number: 28A2024-0A0) and the sensor lines (Part Number: 28A2025-0A2), see Fig. 2c. These ferrite chokes are designed to snap tightly onto the line cables and couple inductively to the system circuitry, subsequently suppressing (choking) frequencies lower than 100 MHz. RF choke additions to the power line and the sensor line were evaluated separately using SNR analysis as described above.

2.5. Electrical grounding of MWG power and sensor lines

The coaxial power and sensor lines connect MWG on one end and MW antenna on the other end. The lines are shielded with the vendor-supplied copper braided sleeve which is also electrically connected to the pin on the grounded chassis of the generator. For MWG location outside the MR scan room (see Fig. 2a and c) the coaxial lines had to be fed into the scan room through the waveguide in the grounded penetration panel. Electrical contact between the coax shielding and the walls of the waveguide was established using layers of copper wool wrapped manually around the cables.

The effect of the grounding on MR image quality was assessed in a series of ten SNR tests collected on separate days (in order to get a better evaluation of consistency of manual grounding). Each test consisted of two sets of SNR measurements performed under two conditions. For the first condition coaxial lines were fed through the waveguide with no particular attention to the grounding. For the second condition grounding was carefully established using copper wool to secure the waveguide and coaxial lines within it. The microwave generator was in the optimal configuration of RF chokes based on the results of the prior testing described above.

2.6. PRFS monitoring of hepatic MWA: manual respiratory gating

As mentioned in the Introduction, MR thermometry in our body ablation practice has been implemented with the aid of a Visualase workstation (Medtronic, Minneapolis, MN), which directly connects to the MRI scanner's computer in the control room via an ethernet cable. The 2D spoiled gradient echo sequence (TR = 20 ms, TE = 12 ms, Flip = 15°, matrix = 256 × 256, FOV = 36 × 36 cm, BW = 90 Hz/Px, slice = 10 mm, acquisition time for each frame = 3 s) was used to collect MR thermometry data. In order to minimize artifacts due to respiration, the acquisition matrix was adjusted to achieve the desired acquisition time and enable manual synchronization with the patient's respiratory cycle. The anesthetist set the patient respiratory cycle to 8–10 breaths per minute at an inspiratory to expiratory ratio between 1:2 and 1:3 (a range of 1.875–2.5 s inspiration and 5–5.625 s expiration for 8 breaths per minute, or 1.5–2 s inspiration and 4–4.5 s expiration

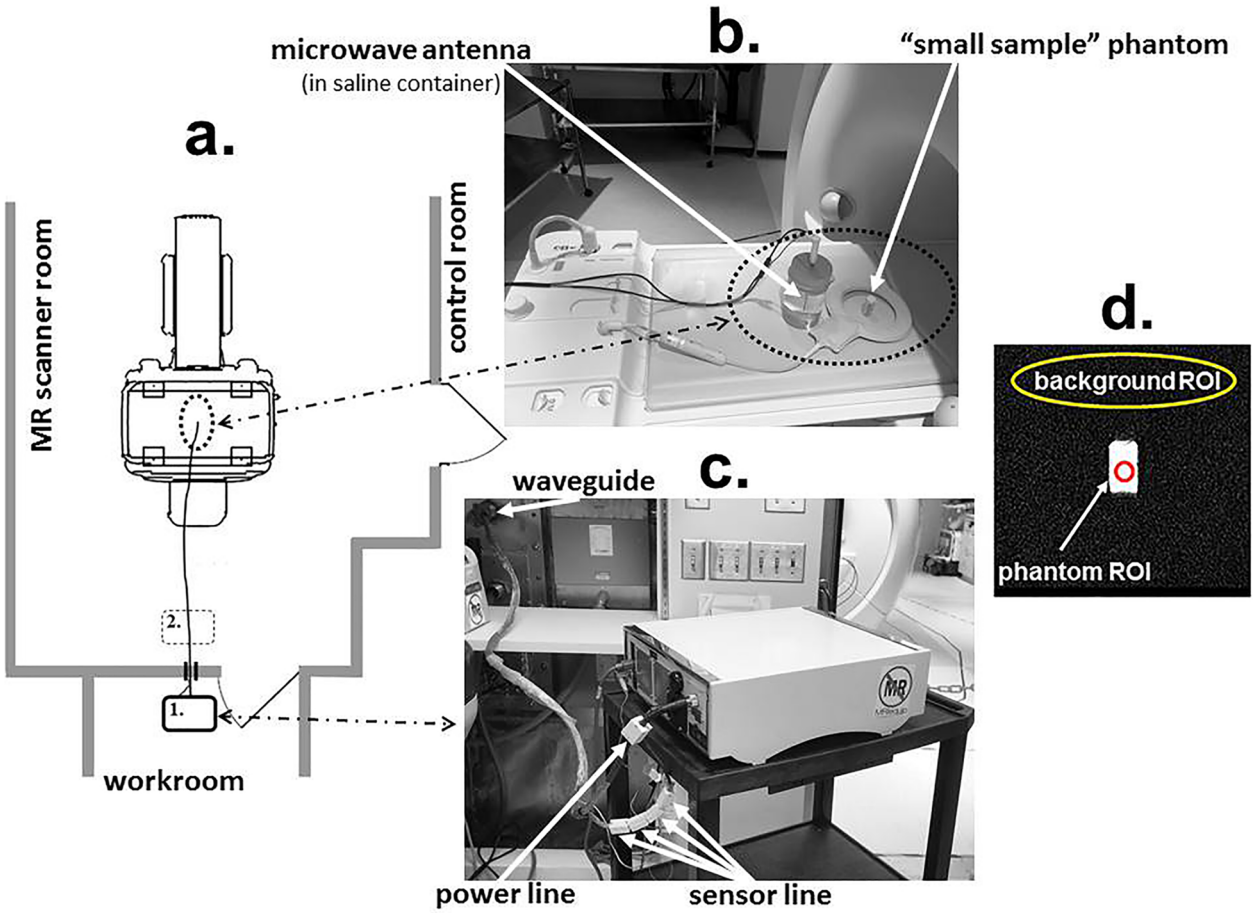

Fig. 2. Experimental setup for optimizing image quality during active microwave ablation. a. Schematic representation of the setup. Microwave generator locations inside the workroom (1) and inside the MR scanner room (2) are shown. The dotted ellipses indicate location of phantom arrangement within the scanner bore. b. Detailed arrangement of the "small sample" phantom inside the clinical flex coil and microwave antenna inserted into a container with saline. c. Microwave generator positioned inside the workroom. RF chokes on the power and sensor lines are indicated with white arrows. d. Schematic representation of the SNR measurement. "Signal" is measured as an average of signal intensities inside the "small sample" phantom ROI, "noise" is measured as a standard deviation of signal intensities inside the background ROI.

for 10 breaths per minute) depending on the patient condition, which allowed sufficient time to acquire one image during expiration. The scanner's "pause" option between every image was selected and the specifically-trained MR technologist (same technologist performed this task for all cases) watched the respiratory bellows on the anesthesia machine inside the scan room to initiate the scan at the beginning of each expiration phase. The resulting acquisition time of the PRFS images was 6–7.5 s. The workstation was set to automatically receive the images from the scanner in every respiratory cycle and the phase images were sequentially displayed. The user determined which image was to serve as a baseline for PRFS thermometry and, subsequently, the MR temperature and the corresponding thermal tissue damage maps were computed and displayed overlaid with anatomical images on the workstation screen.

The first patient treated using this approach had prostate cancer metastasis in the liver, see Fig. 6a. At the start of the procedure the anesthetized and intubated patient was brought into the scan room and positioned supine feet-first on the MRI table. The medium MW antenna was inserted into the tumor: initially with ultrasound-guidance, followed by MR-guidance and MRI-confirmation of the desired antenna location, see Fig. 6b. The ultrasound guidance of antenna insertion was performed inside MR scanner room in a setup described previously in detail by our group [24].

Upon treatment completion Gadolinium (Gd) contrast was administered and contrast-enhanced T1 images were acquired using the volumetric T1-weighted high-resolution field echo sequence (e-Thrive) with the following parameters: TR/TE = 2.0/4.0 ms, Flip = 10°, ETL = 43, matrix = 180 × 180, slice/slice overlap = 5/2.5 mm, FOV = 36 × 36 cm, BW = 434 Hz/Px) to visualize the extent of ablation.

2.7. Assessment of the clinical PRFS thermometry images

The PRFS thermometry images acquired during clinical cases were evaluated post-treatment to assess the SNR reductions caused by the activation of MWG, uncertainty of the temperature measurements, and comparison of thermal lesion dimensions predicted by PRFS and visualized in contrast-enhanced MRI. Similarly to SNR evaluations of equipment modifications described above, the effect of the action of MWG was expressed in terms of the ratio of the SNR measured in magnitude PRFS image just prior to MWG activation to that measured at same location just after MWG activation. The signal was measured as average pixel value from circular ROI placed in the unheated portion of the liver, the noise was measured in the oval ROI placed in air (see Fig. 6c). The uncertainty of the PRFS temperature was determined as standard deviation of temperature history data collected within 3 × 3 pixel ROI placed in the unheated portion of the liver.

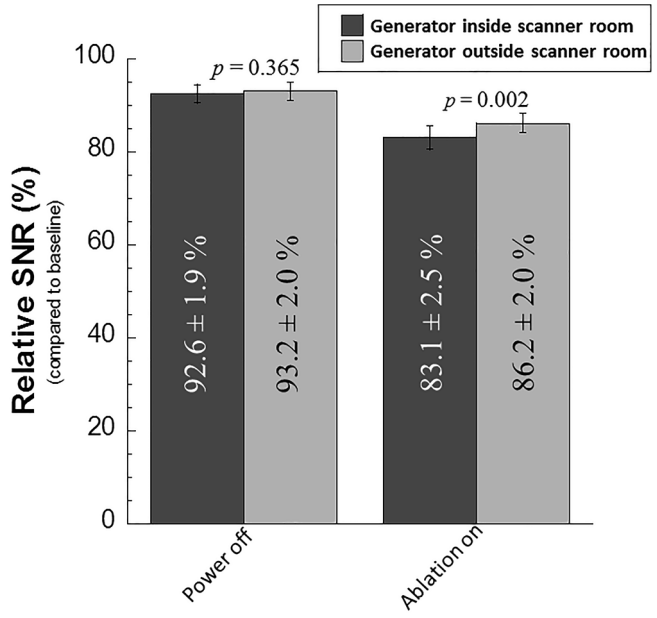

Fig. 3. Image SNR (relative to baseline) versus location of the microwave generator.

3. Results

3.1. MWG location

The location of MWG outside versus the inside of the MR scanner room had similar effect on the MR image SNR, regardless of the system's operational status, see Fig. 3. Positioning the generator outside the scanner room seemed to result in a slight improvement to image SNR relative to location inside the scanner room. Corresponding to "ablation on" operational status, this result was statistically significant ($p = 0.002$; Student's t-test). This result, however, was strongly dependent on the adequate grounding of the coaxial power and sensor lines inside the waveguide (see results shown in a section dedicated to electrical grounding below). Based on the results shown in Fig. 3, MWG location outside the MR scanner room was selected for clinical use.

3.2. Addition of RF chokes

Incremental addition of RF chokes to the power or the sensor lines resulted in similar patterns of SNR improvement, see Fig. 4. Image SNR initially increased with increasing number of RF chokes but eventually leveled off. Additions of more than one RF choke on the Power line and more than four chokes on the Sensor line did not result in significant SNR improvements. Based on the data, the combination of one choke on the Power and four chokes on the Sensor line was selected for clinical use. With that optimized combination, the SNR was improved by a factor of about 68% over the configuration without the chokes.

3.3. Electrical grounding of MWG's power and sensor lines

Adequate grounding of coaxial lines inside the waveguide was found to have a substantial positive effect on the MR image quality, see Fig. 5. The average SNR ratios measured when lines were carefully grounded inside the waveguide were more consistent and increased approximately by the factor of two relative to SNR ratios measured when the lines were simply fed through the waveguide with no attention paid to grounding (0.88 ± 0.08 versus 0.49 ± 0.28, $p = 0.002$). Additionally, poor grounding occasionally resulted in the EMI contamination ("walking" vertical EMI lines moving horizontally between subsequent image frames), which is reflected in increased standard deviations of individual measurements.

Based on the measurements shown in Fig. 5, minimal SNR ratio of 0.72 ($\text{SNR Ratio}_1 - 2 \times$ standard deviation) and absence of EMI, were established as Quality Assurance (QA) criteria to be tested prior to each clinical treatment. The time required for the QA testing process (phantom setup, "baseline" acquisition, feeding/grounding the coaxial lines through the waveguide, image acquisition during generator activation using test antenna) was less than 10 min. This QA process was additionally found to be useful in detecting and troubleshooting of issues other than electrical grounding of the coaxial lines: damaged coaxial line connectors and faulty microwave generator also resulted in severe reductions of SNR ratios (0.22 ± 0.19 and 0.07 ± 0.01, respectively).

3.4. PRFS monitoring of hepatic MWA: manual respiratory gating

Based on the technical assessments, the following equipment configuration was selected for the clinical treatments: microwave generator outside the MR scanner room, one RF choke on the power line, four RF chokes on the sensor line. In addition, based on data shown in Fig. 3, the baseline images for the MR thermometry were acquired with the generator in the "off" mode. During the ablations, although there was still visually appreciable increase in image noise as well as intermittent presence of EMI in MR images, no significant motion artifact or image misalignments were observed. Fig. 5 shows results from the first patient treated using the reported approach. The T2*-weighted signal intensity changes (Fig. 6c), PRFS thermometry (Fig. 6d), and the corresponding dose maps (Fig. 6e) showed the ablation zone with clinically useful image quality. The extents of ablation measured in the thermal damage maps were a good predictor of ablation size found in the T1-weighted images with Gadolinum contrast acquired immediately after treatments (Fig. 6f). The thermometry results using our improvement approach and shown in Fig. 6 were judged to be clinically useful. Our practice has insofar performed five clinical MWA treatments with similar results with regard to MR image quality.

3.5. Evaluation of the clinical PRFS thermometry images

Our practice has insofar performed five clinical MR-guided MWA treatments. One of the five patients, however, denied use of their data for research and publication purposes. The remaining treatments are represented in Fig. 7. Results of the evaluation of clinical PRFS images of all four cases are summarized in Table 1.

4. Discussion

This work demonstrated that practical and non-invasive modifications to the use and configuration of the Avecure microwave system can achieve robust PRFS image quality sufficient for guiding clinical ablations. Furthermore, synchronization of the image acquisition with the patient respiratory cycle was shown to sufficiently limit respiratory-motion artifact observed previously in temperature and dose maps (Fig. 1B versus Fig. 6d, and e). The method of manual synchronization has the advantage of simplicity, and is also very robust in our experience (which may be due to the fact that it was performed by a single trained operator only). It may however be also labor-intensive, requiring continuous attention of the technologist to synchronization of MRI scans with the cycle of respiratory bellow on the anesthesia machine. For these reasons, the automated synchronization methods such as respiratory-gating or triggering [17,25], or application of the reference-less PRFS thermometry [26] may be preferable. However, the respiratory triggering in our existing thermometry sequence only allowed one k-space line to be acquired after each trigger and was therefore, not useful. Reference-less PRFS could also improve the robustness of MR thermometry to motion by removing the need of a reference image, although thermal dose calculation could still be

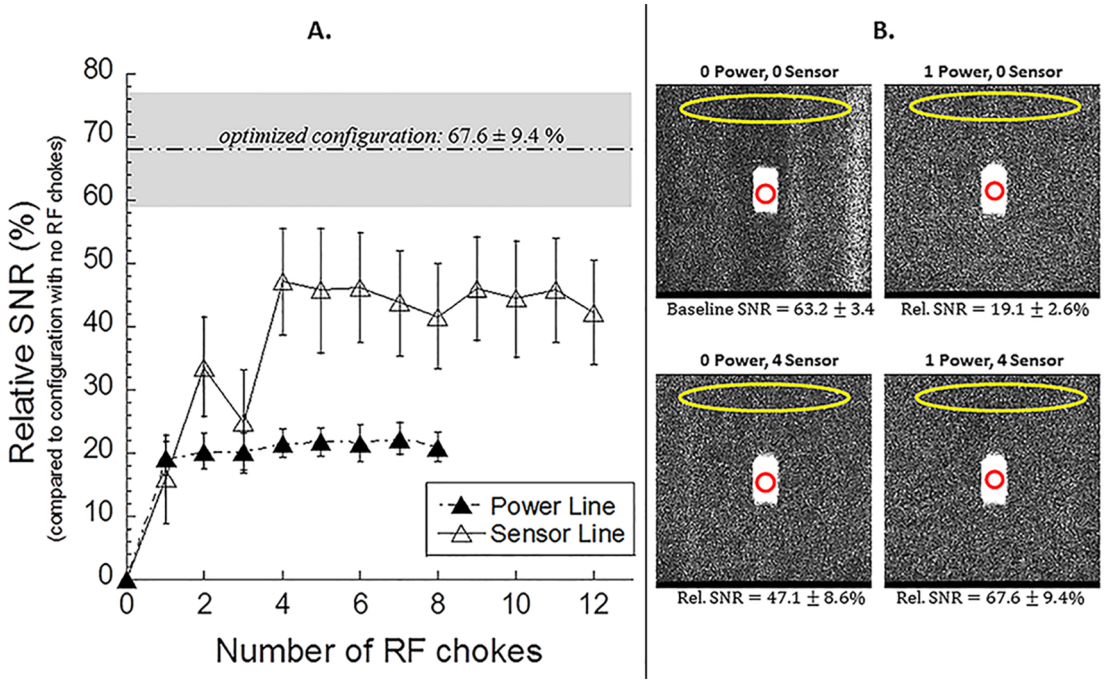

Fig. 4. Image SNR versus number of ferrite RF chokes on power and sensor lines. Based on the data, the optimal configuration of one choke on Power and four chokes on Sensor coaxial lines was selected for the clinical treatment (SNR corresponding to this configuration is also shown). Shaded band visualizes the standard deviation of measurements using the optimized configuration.

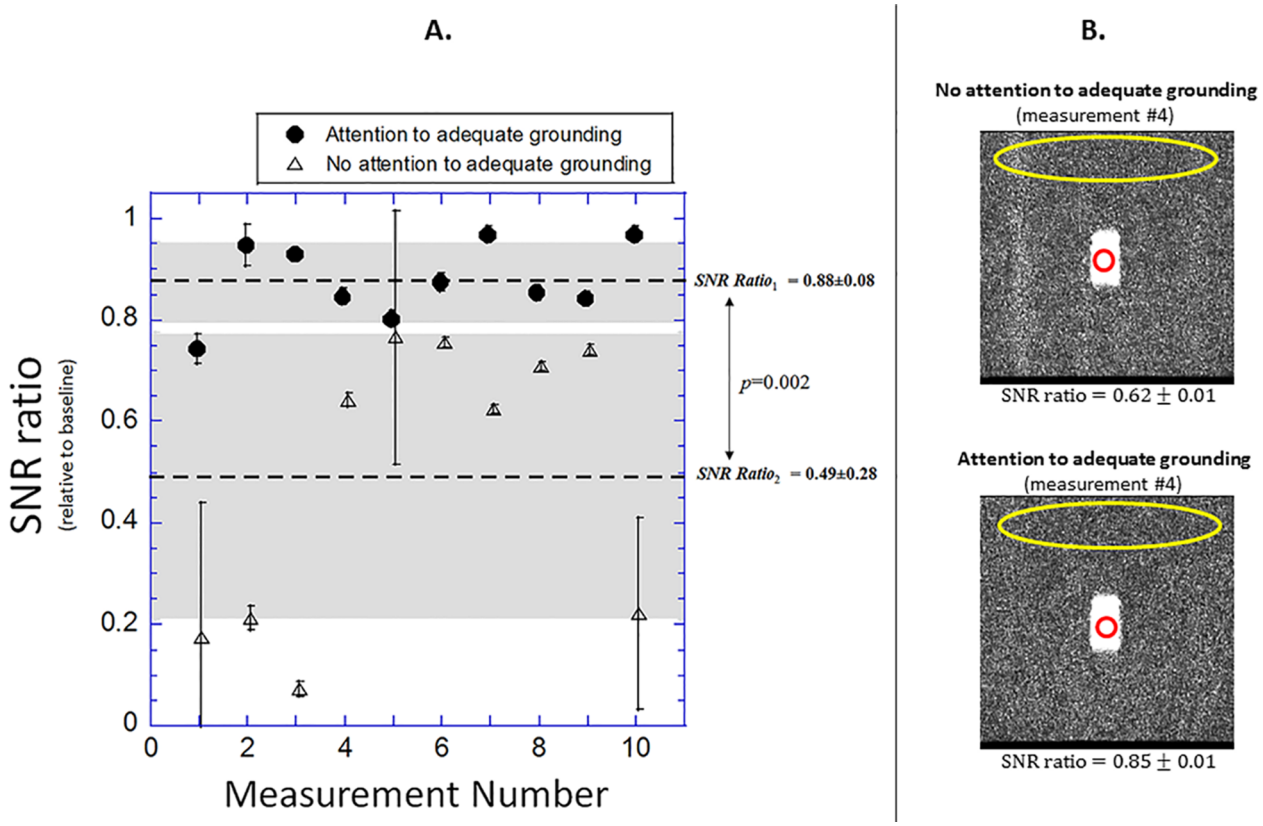

Fig. 5. SNR ratio testing of electrical grounding of microwave generator's coaxial lines fed into MR scan room via the waveguide. When attention was paid to careful grounding using copper wool, the average ratio was 0.88 ± 0.08, which was significantly higher than 0.49 ± 0.28 corresponding to feeding coaxial lines without paying attention to grounding. The difference was statistically significant ($p = 0.002$, Student's *t*-test). Large standard deviations of individual measurements reflect presence of "walking" EMI. The shaded bands indicate standard deviations of the SNR ratio averages.

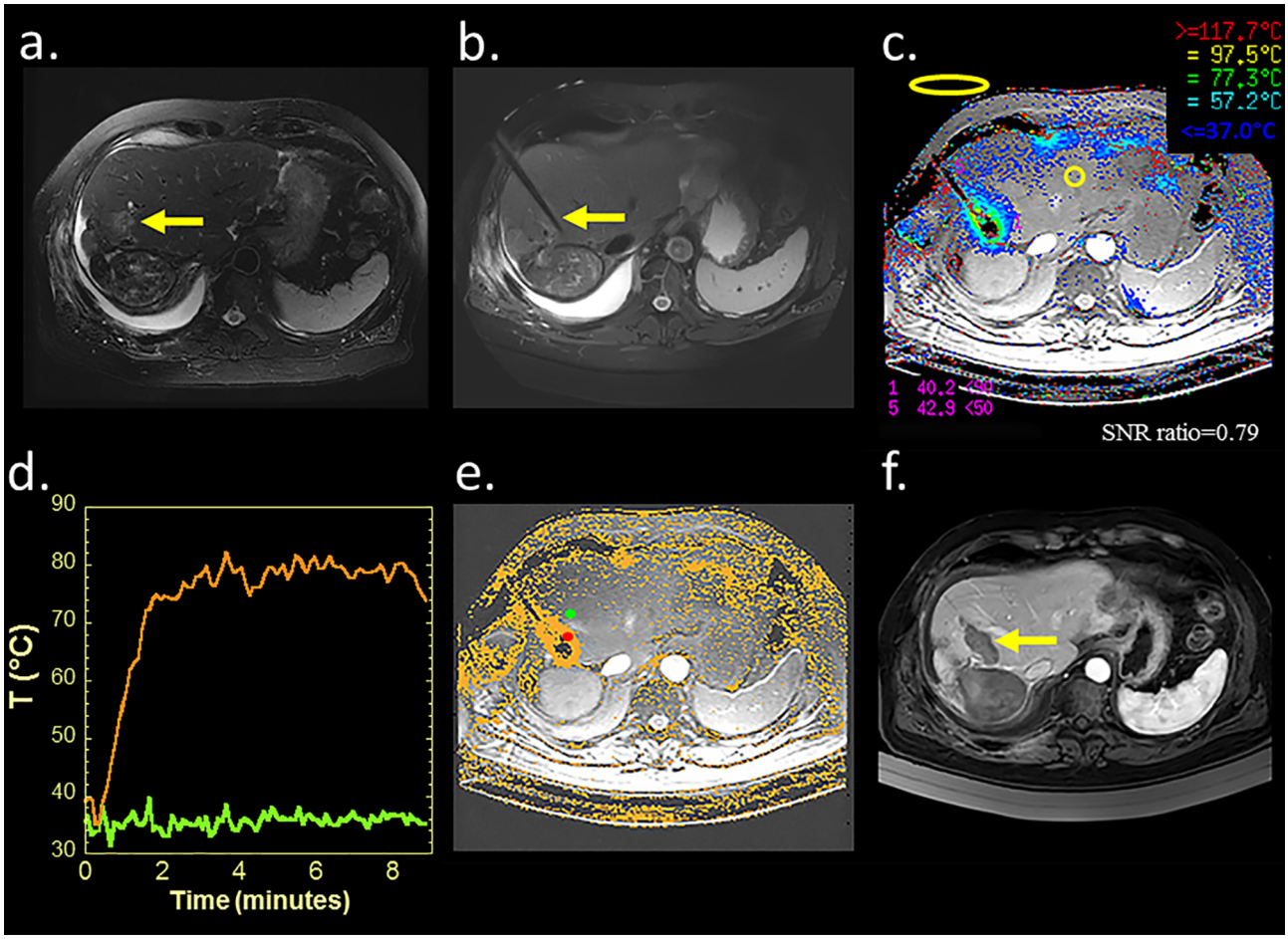

Fig. 6. MR-guided MWA in the male patient with hepatic prostate cancer metastases. a. Axial T2 image with fat saturation showing targeted tumor (arrow). b. Axial T2 image confirming adequate placement of the microwave antenna introducer into target tissue (arrow). c. Final frame of the PRFS thermometry imaging sequence showing temperature elevations around the target site after 8 min and 10 s MWA. The yellow circular and oval ROI's indicate locations of the signal and noise measurements (before and after MWG activation), respectively. d. Example temperature histories sampled over 3 × 3 pixel ROI's placed within the ablated volume and in the unheated liver region in the vicinity of ablation site (red and green dots in frame e, respectively). e. Thermal damage overlay (orange). f. Post-ablation axial contrast-enhanced T1 image showing ablation lesion (arrow). (For interpretation of the references to color in this figure legend, the reader is referred to the web version of this article.)

degraded by motion if data acquisition is not synchronized to the same respiratory phase. Automatic methods for mitigating respiratory-motion artifact that combine the advantages of these methods are currently being investigated for future comparison with the manual synchronization.

Because the Avecure microwave generator assembly contains ferrous components, the generator location outside the scanner room is our strongly-preferred choice, since it eliminates the risk of accidental magnetic displacement inside the busy environment of the MR scanner room during clinical ablations (numerous clinical personnel, anesthesia equipment, carts with surgical supplies, etc.). This location is also superior from the standpoint of the clinical workflow, since it does not require the generator's operator to be present inside the MR scanner room which requires the use of ear protection, thereby, allowing for safer and easier communication with the treating physician. Prior to testing of any ferrous devices inside the MR scan rooms, it is extremely important to evaluate magnetic field and spatial magnetic field gradients at the proposed use location and along the route of introduction. Our assessments of the magnetic field inside the scanner room followed the protocol applied previously to a compact ultrasound scanner [24]. We also labeled the generator according to the recommendation of the American College of Radiology [28] and ensured it was handled by the trained personnel.

Our experiments have shown that in the outside location a great deal of attention must be paid to the adequate grounding and shielding of the coaxial lines connecting the antennae through the grounded penetration panel. A good indicator of inadequate grounding, when lines are passed through the waveguide, is increased noise and electromagnetic interference associated with the outside location (versus the inside). After ensuring the lines are well-shielded and grounded to both the generator chassis and the penetration panel, the noise and EMI levels associated with location outside the scanner room improved to a point of being equivalent or even slightly superior to those corresponding to location inside the MR scanner room. As the levels of electronic noise and the amount of EMI present strongly depend on the grounding of the coaxial lines inside the waveguide, the DQA testing prior to every treatment is paramount. The QA procedure presented in this manuscript has been shown to be both expeditious (less than 10 min) and adequate for assessment of any potential imaging issues.

Following the technical improvements presented herein, the reductions of SNR seen in clinical patient images (14% average), listed in Table 1, were consistent and closely matched the acceptance levels as measured during our QA testing in a phantom in a fixed geometry. Despite this successful improvement of MR image SNR and reduction of respiratory motion artifacts, the images acquired during the ablation, still occasionally suffered from small but appreciable amount of noise and EMI associated with the action of the MWG. Furthermore, in our experience when the EMI was present it also tended to increase in

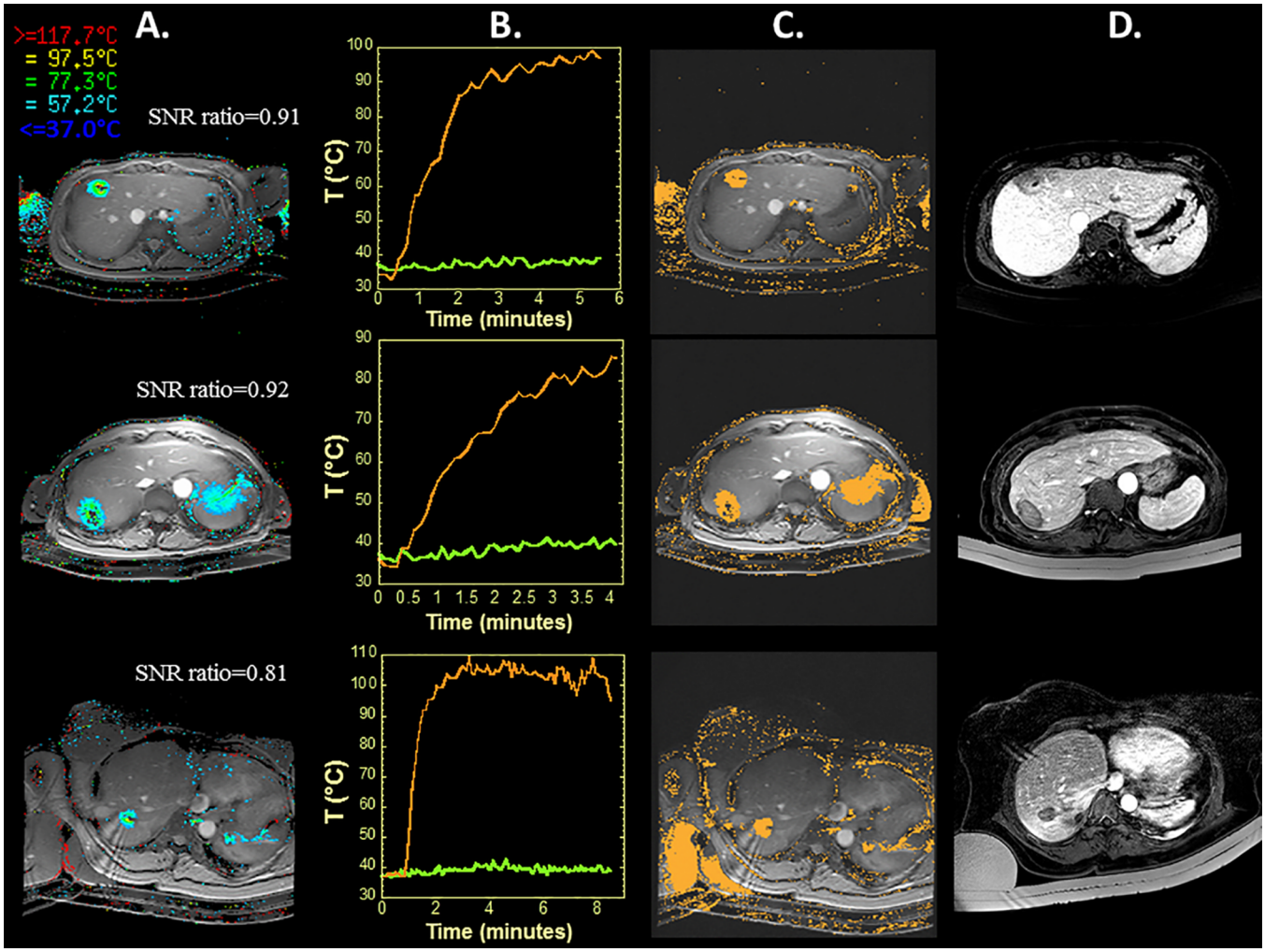

Fig. 7. Representation of the PRFS thermometry during three additional MWA patient cases. Column A. Final PRFS thermometry frames showing temperature elevations around target sites. "SNR ratios" of SNR measured at MWG activation, divided by SNR measured prior to MWG activation are also shown. Column B. Temperature histories sampled from 3 × 3 voxel ROI's placed within the ablation zones and within unheated regions of the liver in the vicinity of ablation zone. Column C. Thermal tissue damage overlays (orange). D. Post-ablation axial T1 with gadolinium contrast showing non-perfused ablation lesions. Top row: 5 min 6 s MWA, carcinoid metastasis. Middle row: 3 min 50 s MWA, recurrent hepatocellular carcinoma. Bottom row: 7 min 28 s MWA, colorectal metastases. (For interpretation of the references to color in this figure legend, the reader is referred to the web version of this article.)

intensity towards the end of ablations, as tissue properties changed (potential limitation of our QA testing using saline is that saline's properties remain constant during the MWG activation), occasionally still degrading the dose information. One potential approach to mitigate image quality degradation due to EMI is to interleave the ablation with MRI data acquisition, i.e., only acquiring MRI thermometry images when the microwave is temporarily powered off or in stand-by mode [22]. This approach, however, can potentially compromise the

Table 1
Analysis of PRFS images shown in Figs. 6 and 7. Columns 2 and 3: SNR values measured in PRFS images prior and just after activation of microwave generator (measurement is illustrated in Fig. 6c. Column 4: Ratio of the values in Column 3 over those in Column 2. Column 5: temperature uncertainty (i.e. standard deviation in measured temperature increase at the ablation site at the end of ablation cycle). Column 6: size of thermal lesion (in two orthogonal dimensions) measured in thermal damage maps and contrast-enhanced MRI (in parentheses).

Pt. case	SNR		SNR ratio	Temperature uncertainty ΔT (°C)	Lesion size (mm^2) PRFS (T1 with Gd)
	MWG off	MWG on			
Fig. 6	61.3	48.7	0.79	± 1.2	27.1 × 46.4 (22.8 × 43.0)
Fig. 7 top row	28.2	25.9	0.92	± 1.4	27.0 × 25.3 (23.4 × 19.1)
Fig. 7 middle row	30.4	24.6	0.81	± 1.6	41.5 × 27.2 (39.0 × 21.8)
Fig. 7 bottom row	72.2	66.2	0.92	± 1.3	27.0 × 25.3 (23.4 × 19.1)
			Average	± 1.4	

treatment effectiveness and complicate synchronization of MRI with respiratory cycle and is therefore currently not preferred by our physicians. Advanced real-time image processing methods to further mitigate the noise introduced into MR images by the microwave system are currently under investigation.

The overall uncertainty in temperatures found in patient data was on the order of ± 1.4 °C, which is consistent with the values reported in literature [29]. The limitations of the PRFS thermometry approach used in our treatments include: the inherent temperature uncertainty (determined as standard deviation of temperature estimate), due to combined effects from tissue motion, fat fraction, and MR system instability during MWA (e.g. field drifts and thermal noise. Field drifts are most likely responsible for consistent underestimation of lesion sizes listed in Table 1. This phenomenon has been widely reported on in the literature [12,29–32] and several methods have been proposed to mitigate it for improved accuracy of PRFS [33,34]. Real-time corrections for field drifts at the ablation site are currently being investigated by our group. In addition to the above limitations, the ablity to visualize thermal changes near the tip of the microwave antenna is further affected by the blooming hypointense artifact seen around the antenna in Fig. 6d. This artifact can be attributed to a combination of intra-voxel spin dephasing caused by steep and rapid temperature elevations [35], changes in T1 and T2 relaxation times caused by tissue heating [23], and/or steam propagating backwards along antenna shaft. Finally, fat suppression was not used in these five cases, which may have contributed further to temperature uncertainty in areas of elevated fat content. As of now, use of fat suppression in MR monitoring of hepatic ablations has not been widely implemented partially due to concerns of reducing SNR and increasing scan times [12,30–32]. Due to these concerns the clinical decision was made to not use fat suppression. Implementation of approaches minimizing standard deviation of temperature estimate and utilizing fat suppression techniques are the subject of current investigations.

5. Conclusion

A practical procedure to achieve non-invasive equipment modifications and effective acquisition methods resulting in robust and reliable real-time MR thermometry for monitoring of clinical hepatic microwave ablations is described. These modifications to the equipment and workflow needed to take into account the significant and important clinical constraints. Furthermore, a routine QA testing (prior to every treatment) procedure which was developed specifically for MR-guided MWA procedures was to provide an assurance of consistent image quality and high quality patient treatments.

References

[1] Lubner MG, Brace CL, Hinshaw JL, Lee FT. Microwave tumor ablation: mechanism of action, clinical results and devices. J Vasc Interv Radiol 2010;21(8 Suppl):S192–203.

[2] Simon CJ, Dupuy DE, Mayo-Smith WW. Microwave ablation: principles and applications. Radiographics 2005;25(Suppl 1):S69–83.

[3] Seki T, Wakabayashi M, Nakagawa T, Itho T, Shiro T, Kunieda K, et al. Ultrasonically guided percutaneous microwave coagulation therapy for small hepatocellular carcinoma. Cancer 1994;74(3):817–25.

[4] Li X, Fan WJ, Zhang L, Zhang XP, Jiang H, Zhang JL, et al. CT-guided percutaneous ablation of liver metastases from nasopharyngeal carcinoma. J Vasc Interv Radiol 2013;24(5):680–4.

[5] Filippiadis DK, Spiliopoulos S, Konstantos C, Reppas L, Kelekis A, Brountzos E, et al. Computed tomography-guided percuntaneous microwave ablation of hepatocellular carcinoma in challenging locations: safety and efficacy of high-power microwave platforms. Int J Hyperthermia 2017;3:1–7.

[6] Clasen S, Pereira PL. Magnetic resonance guidance for radiofrequency ablation of liver tumors. J Magn Reson Imaging 2008;27:421–33.

[7] Hoffmann R, Rempp H, Keßler DE, Weiß J, Pereira PL, Nikolau K, et al. MR-guided microwave ablation in hepatic tumors: initial results in clinical routine. Eur Radiol. 2017;27(4):1467–76.

[8] Solbiati L, Ierace T, Goldberg SN, et al. Percutaneous US-guided radio-frequency tissue ablation of liver metastases: treatment and follow-up in 16 patients. Radiology 1997;202:195–203.

[9] Leydendecker JR, Dodd 3r GD, Halff GA, et al. Sonographically observed echogenic response during intraoperative radiofrequency ablation of cirrhotic livers pathologic correlation. AJR Am J Roentgenol 2002;178:1147–51.

[10] Cha CL, Lee FT, Gurney JM, Markhardt BK, Warner TF, Kelcz F, et al. CT versus sonography for monitoring radiofrequency ablation of porcine liver. AJR Am J Roentgenol 2000;175:705–11.

[11] Park MH, Rhim H, Kim YS, Choi D, Lim HK, Lee WJ. Spectrum of CT findings after radiofrequency ablation of hepatic tumors. Radiographics 2008;28:379–90.

[12] Rieke V, Butts Pauly K. MR thermometry. J Magn Reson Imaging 2008;27:376–90.

[13] Sapareto SA, Dewey WC. Thermal dose determination in cancer therapy. Int J Radiat Oncol Biol Phys 1984;10:787–800.

[14] Tempany CM, Stewart EA, McDannold N, Jolesz FA, Hynynen K. MR imaging-guided focused ultrasound surgery of uterine leiomyomas: a feasibility study. Radiology 2003;226(3):897–905.

[15] Carpentier A, McNichols RJ, Stafford RJ, Itzcovitz J, Guichard JP, Reizine D, et al. Real-time magnetic resonance-guided laser thermal therapy for focal metastatic brain tumors. Neurosurgery 2008;63(1 Suppl 1):ONS21-8.

[16] Lepetit-Coiffe M, Laumonier H, Seror O, Quesson B, Sesay MB, et al. Real-time monitoring of radiofrequency ablation of liver tumors using thermal-dose calculation by MR temperature imaging: initial results in nine patients, including follow-up. Eur Radiol 2010;20:193–201.

[17] Rempp H, Hoffmann R, Roland J, Buck A, Kickhefel A, et al. Threshold-based prediction of the coagulation zone in sequential temperature mapping in MR-guided radiofrequency ablation of liver tumours. Eur Radiol 2012;22:1091–100.

[18] Morikawa S, Inubushi T, Kurumi Y, Naka S, Sato K, Tani T, et al. MR-guided microwave thermocoagulation therapy of liver tumors: initial clinical experiences using a 0.5T open MRI system. J Magn Reson Imaging 2002;16:576–83.

[19] Kurumi Y, Tani T, Naka S, Morikawa S, Inubushi T, Seshan V. Clinical experiences with MR-guided microwave ablation for liver tumors. Proc Intl Soc Mag Reson Med 2001;9:2204.

[20] Dong J, Zhang L, Li W, Mao S, Wang Y, Wang D, et al. 1.0T open-configuration magnetic resonance-guided microwave ablation of pig livers in real time. Sci Rep 2015;5:13551. https://doi.org/10.1038/srep13551.

[21] Demura K, Morikawa S, Murakami K, Sato K, Shiomi H, Naka S, et al. An easy-to-use microwave hyperthermia system combined with spatially resolved MR temperature maps: phantom and animal studies. J Surg Res 2006;135:179–86.

[22] Kaltenbach B, Roman A, Eichler K, Nour-Eldin A, Vogl TJ, Zangos S. Real-time qualitative MR monitoring of microwave ablation in ex vivo livers. Int J Hyperthermia 2016;32(7):757–64.

[23] Rosenberg C, Kickhefel A, Mensel B, Pickartz, Puls R, Roland J, Hosten N. PRFS-based MR thermometry versus alternative T1 magnitude method – comparative performance predicting thermally induced necrosis in hepatic tumor ablation. PLOS ONE 2013;8(10):1–11.

[24] Ma C, Long Z, Lanners DM, Tradup DJ, Brunquell CL, Felmlee JP, et al. Protocol for testing suitability of compact US imaging systems for use inside MRI suites, and application to one commercial US system. Biomed Phys Eng Express 2016;2(4):047003.

[25] Vigen KK, Daniel BL, Pauly JM, Butts K. Triggered, navigated, multibaseline method for proton resonance frequency temperature mapping with respiratory motion. Magn Reson Med 2003;50:1003–10.

[26] Rieke V, Vigen KK, Sommer G, Daniel BL, Pauly JM, Butts K. Referenceless PRF shift thermometry. Magn Reson Med 2004;51:1223–31.

[27] Chen JC, Moriarty JA, Derbyshire JA, Peters RD, Trachtenberg J, Bell SD, et al. Kucharczyk W. Prostate cancer: MR imaging and thermometry during microwave thermal ablation-initial experience. Radiology 2000;214(1):290–7.

[28] Kanal E, Barkovich AJ, Bell C, et al. ACR guidance on MR safe practices. J Magn Reson Imaging 2013;37:501–30.

[29] Ishihara Yasutoshi, et al. A precise and fast temperature mapping using water proton chemical shift. Magn Reson Med 1995;34(6):814–23.

[30] Yuan J, Mei CS, Panych LP, McDannold NJ, Madore B. Towards fast and accurate temperature mapping with proton resonance frequency-based MR thermometry. Quant Imaging Med Surg. 2012;2(1):21–32.

[31] De Poorter J, De Wagter C, De Deene Y, et al. Noninvasive MRI thermometry with the proton resonance (PRF) method: in vivo results in human muscle. Magn Reson Med 1995;33:74–81.

[32] McDannold N. Quantitative MRI-based temperature mapping based on the proton resonant frequency shift: review of validation studies. J Hyperthermia 2005;21(6):533–46.

[33] Hernandez D, Kim KS, Michel E, Lee SY. Correction of B0 drift effects in magnetic resonance thermometry using magnetic field monitoring technique. Concepts Magn Reson Part B 2016;46B(2):81–9.

[34] Chen Y, Ge M, Ali R, Jiang H, Huang X, Qiu B. Quantitative MR thermometry based on phase-drift correction PRF shift method at 0.35T. Biome Eng Online 2018;17(1):39.

[35] Arvanitis CD, McDannold N. Integrated ultrasound and magnetic resonance imaging for simultaneous temperature and cavitation monitoring during focused ultrasound therapies. Med Phys 2013;40(11):1–14.